Clays and Clay Minerals, Vol. 56, No. 6, 645–654, 2008.

TRANSFORMATION OF SYNTHETIC Zn-STEVENSITE TO Zn-TALC INDUCED BY THE HOFMANN-KLEMEN EFFECT

S. PETIT*, D. RIGHI, AND A. DECARREAU

Université de Poitiers, FRE3114 CNRS, HydrASA, 40 Avenue du Recteur Pineau, F-86022 POITIERS Cedex, France

Abstract—Stevensite-like sauconite, with the general composition: Si_4 $(Zn_{3-x}\square_x)O_{10}(OH)_2R^+_{2x}$, where $\square$ is a vacant site, was synthesized. The objective was to study the possible migration of some cations (Li^+ and Zn^{2+}) within such trioctahedral smectites, under heating, following the so-called 'Hofmann-Klemen' (HK) effect. The initial gel was divided into five aliquots and placed in teflon-coated hydrothermal reactors with distilled water, and these were hydrothermally treated at 80, 100, 120, 150, and 200ºC, respectively, over 30 days. X-ray diffraction (XRD) analysis confirmed that the samples synthesized were smectites. The number of vacant sites (x) per half unit cell ($O_{10}(OH)_2$) ranged from nearly 0 to 0.23 but no simple relationship was established between x and the temperature of synthesis. The samples were Li^+- and Zn^{2+}-saturated, and heated overnight at 300ºC (HK treatment). Cation exchange capacity measurements were made by Fourier transform infrared spectroscopy (FTIR) on NH_4^+-saturated samples. After LiHK treatment, the structural formula of samples could be expressed as: $Si_4Zn_{(3-x)}Li_xO_{10}(OH)_2NH_{4x}^+$, while after ZnHK treatment, it could be expressed as: $Si_4Zn_3O_{10}(OH)_2$. Analysis by XRD and FTIR showed that the samples moved from a Zn-stevensite-like structure to Zn-talc-like structure after treatment with ZnHK. These results are interpreted as evidence that Zn^{2+} (and Li^+) migrated into the previously vacant sites under HK treatment.

Key Words—Cation Exchange Capacity, Hofmann-Klemen, Kerolite, Li^+, NH_4^+, Octahedral Charge, Sauconite, Smectite, Stevensite, Synthesis, Zinc.

INTRODUCTION

Sauconite is the general name given to the Zn-rich members of the smectite group. The name comes from the first discovery of the mineral at the Uberroth Mine in the Saucon Valley, Pennsylvania (Genth, 1875). Sauconite found in nature generally has a saponite-like, Zn-rich smectite structure, *i.e.* with tetrahedral charge due to Al/Si substitutions in tetrahedral sheets (Ross, 1946; Faust, 1951). Sauconite usually occurs in the oxidation zone of Zn deposits, occasionally associated with hemimorphite ($Zn_4Si_2O_7(OH)_2H_2O$) and smithsonite ($ZnCO_3$). It also occurs in the oxidation zone of some sulfide ore bodies together with willemite (Zn_2SiO_4) and hemimorphite (Tiller and Pickering, 1974). Its geological occurrence suggests formation by weathering, and therefore may have implications for the chemistry of Zn in soils and sediments. The occurrence of anthropogenic Zn in soils due to industry (dusts emissions) and the spreading of contaminated wastes (sewage sludge, slurry, dredged sediments) has become an environmental problem (*e.g.* Mench *et al*., 2000). Recent studies have shown that Zn-bearing phyllosilicate is the most common secondary Zn-rich mineral formed by weathering in temperate climate areas (*e.g.* Isaure *et al*., 2005). Determining the Zn status in phyllosilicates (sorbed or substituted in dioctahedral or trioctahedral structure) is important from geochemical and environmental standpoints. Knowing more about the crystallization conditions of Zn silicates is thus of interest in order to assess the effect of physicochemical parameters on the fate of Zn. A review of the synthesis of smectites (Kloprogge *et al*., 1999) showed that only a small number of studies on the synthesis of Zn-smectites have been undertaken. Early experimental works were carried out at low temperature (100ºC) and atmospheric pressure (Esquevin, 1955, 1956, 1960; Tiller and Pickering, 1974; Leggett, 1978), or at higher temperatures (130−730ºC) and pressures (35−276 bar) (Roy and Mumpton, 1956). More recently, Higashi *et al*. (2002) performed hydrothermal syntheses of saponite-like sauconite with composition $(Si_{3.6}Al_{0.4})Zn_3O_{10}(OH)_2Na_{0.4}^+$ and hectorite-like sauconite with composition $Si_4(Zn_{2.6}Li_{0.4})O_{10}(OH)_2Na_{0.4}^+$. The temperature of syntheses ranged from 100 to 250ºC for 3 to 7 days.

Stevensite-like sauconite with the general composition: $Si_4(Zn_{3-x}\square_x)O_{10}(OH)_2R_a^+$, where $\square$ is a vacant site and a is the octahedral charge ($a = 2x$) was synthesized in the present study. The possible migration of some cations (Li^+ and Zn^{2+}) within such trioctahedral smectites under heating, according to the so-called 'Hofmann-Klemen' (HK) effect (Hofmann and Klemen, 1950), was then studied.

MATERIALS AND METHODS

Materials

Syntheses were performed starting from a gel with a controlled chemical composition. The initial gel was prepared following the procedure described by

* E-mail address of corresponding author:
Sabine.Petit@univ-poitiers.fr
DOI: 10.1346/CCMN.2008.0560605

Decarreau (1985) using 0.1 M sodium metasilicate ($SiO_2Na_2O.5H_2O$) and 0.3 M zinc sulfate ($ZnSO_4.7H_2O$), according to the theoretical precipitation reaction:

$$4SiO_2.Na_2O + 3ZnSO_4 + H_2SO_4 \rightarrow Si_4Zn_3O_{11} + 4Na_2SO_4 + H_2O$$

After precipitation, the solid phase was centrifuged and washed with distilled water to remove as much sodium sulfate as possible. The gel was then divided into five aliquots (~400 mg of hydrated gel) and placed in teflon-coated hydrothermal reactors with 30 mL of distilled water. Each run corresponded to one temperature of the hydrothermal treatment (80, 100, 120, 150, and 200ºC; Table 1). Above 100ºC, the pressure was equal to the vapor-saturation pressure. For all the experiments, the duration of the synthesis period was 30 days and the initial pH was 6.3.

At the end of experiments, the synthesized products were filtered, washed, dried, and ground gently. About 220 mg of sample was obtained for each run. The pH of each material, at the end of the experiment (Table 1), showed only slight variations from the initial pH.

The Hofmann-Klemen treatments consisted of heating Li^+- and Zn^{2+}-saturated samples overnight at 300ºC in a platinum crucible. The LiHK and ZnHK attributes were then added to the name of the Li^+- and Zn^{2+}-treated samples, respectively. Li^+- and Zn^{2+}-saturations were performed using Li- and Zn-chlorides (1 mol dm^{-3}). Suspensions were allowed to stand for 24 h, then centrifuged. The supernatant was removed and the procedure was repeated three times.

Cation exchange capacity (CEC) is the sum of accessible permanent charge and variable charge. Variable charge is due to edge-surface species and is pH-dependent, while the permanent charge is a structural charge. The amount of permanent charge is independent of the amount of variable charge. However, the contribution of variable charge to CEC values is often given as a percentage, *e.g.* a 20−30% contribution of variable charge to the CEC value is considered as a maximum for smectite (Czimerová *et al*., 2006). For stevensite-like smectites, the entire permanent charge is located in the octahedral sheet, is accessible, and is due to the occurrence of vacant sites compared to a talc structure. Isomorphic substitutions of divalent octahedral cations by monovalent Li, as in hectorite, also contribute to permanent charge.

Table 1. Conditions of synthesis.

Sample	*T* (ºC)	pH	CEC
Zn80	80	6.8	–
Zn100	100	5.7*	50.0
Zn120	120	6.9	–
Zn150	150	6.3	–
Zn200	200	6.1	35.0

T: temperature of synthesis.
pH: pH of the quenched end of synthesis fluid.
CEC: cation exchange capacity (Mg saturation measurement) (cmole kg^{-1})
–: not measured
*: a significant loss of fluid was observed.

Layer charge may be estimated from stoichiometric coefficients in structural formulae. Using the molecular weight of the anhydrous compounds such as $Si_4Zn_{(3-x)}\square_xO_{10}(OH)_2NH^+_{4a}$, the following relationship was calculated between the layer charge *a*, in equivalent charges per half unit cell ($O_{10}(OH)_2$), and its corresponding amount of permanent charge (CEC_{perm}) expressed in cmol/kg:

$$a = 0.0049*CEC_{perm} \quad (1)$$

The CEC was measured for all samples (untreated and Li- and Zn-HK-treated) following the method described by Petit *et al*. (1998, 2006) because it needs only a small amount of sample. This method consists of measuring the amount of ammonium in NH^+_4-saturated samples using the $\upsilon_4NH^+_4$ IR vibration band near 1400 cm^{-1}. Samples were NH^+_4-saturated using 1 M ammonium acetate solution. Suspensions of the samples in ammonium acetate solution were obtained by agitation and then left to stand for 2 h. After centrifugation, the samples were removed from solution and the procedure applied once again. The samples were then washed until free of ammonium salts (no reaction with the Nessler reagent). The NH^+_4 contents were measured in arbitrary units (integrated intensities of IR bands) and a 10% error on the measurement was estimated for the Zn100 sample which was available in sufficient amounts (n = 10). This 10% error was used for uncertainties in CEC_{NH4} measured for all samples and is probably overestimated for the samples with greater NH^+_4 contents. To express the measured NH^+_4 contents from arbitrary units into cation quantities by sample mass in cmol/kg, at least one CEC measurement has to be carried out independently by another technique (Petit *et al*., 1998, 2006). This was done for the two samples available in slightly larger amounts (Table 1), using the method described by Righi *et al*. (1993). The samples were saturated with Mg^{2+} and the excess $MgCl_2$ was washed out carefully using ethanol. Mg^{2+} was then replaced by NH^+_4 and analyzed by atomic absorption spectroscopy (AAS) in the exchange solution. In fact, for conversion, only the CEC value measured for Zn100 was used because Zn200 was shown to be impure.

Analytical procedures

X-ray diffraction (XRD) patterns were obtained using a Philips PW-1050/25 DY 5249 diffractometer equipped with Ni-filtered CuKα radiation (40 kV, 40 mA), combined with a SOCABIM system (DACO-MP) for numerical-data acquisition.

A thermobalance NETZSCH STA 409 EP was used for thermal analyses (differential thermal-thermogravimetric analysis: DTA-TG). The measurements were performed on samples of ~20 mg, heated from 20 to 1100ºC, at 10ºC/min in air. The temperature of smectite dehydroxylation was measured at the maximum of the second endotherm. The TG analyses allowed a rough approximation of the rate of smectite crystallization (%cryst, Table 2) by comparing the water loss during dehydroxylation (wt.%) of the anhydrous synthesized sample with the calculated theoretical water loss it should produce in the case of dehydroxylation of pure anhydrous smectite. The calculated theoretical water loss during dehydroxylation of pure anhydrous smectite with a $Si_4Zn_{(3-x)}O_{10}(OH)_2Zn_x$, formula unit and a molar mass of 502.5 g is 3.58%. Thus, the rate of smectite crystallization (%cryst) could be calculated following the equation:

$$\%cryst = \%OH_{anh}/3.58 \quad (2)$$

where $\%OH_{anh}$ is the water loss due to dehydroxylation of the anhydrous synthesized compound.

$$\%OH_{anh} = (1 - \%H_2O/100)*\%H_2O \quad (3)$$

where %OH is the water loss during dehydroxylation (wt.%) measured by TG within the temperature range 250−700ºC (%OH, Table 2), and $\%H_2O$ is the water loss during dehydration measured by TG from 20 to 220ºC ($\%H_2O$, Table 2).

Fourier transform infrared (FTIR) spectra were recorded with a 4 cm^{-1} resolution in transmission mode in the 4000−400 cm^{-1} range using a Nicolet 510 FTIR spectrometer which was purged continuously with dry air containing substantially less CO_2 than normal air. Spectra were obtained from pressed KBr pellets. These pellets, 2 cm in diameter, were prepared by mixing 3 or 4 mg of sample with 300 mg of KBr in order to obtain well defined spectra. Integrated intensities of the absorption bands were achieved using the *OMNIC* software supplied with the Nicolet instrument.

The FTIR spectroscopy was used not only for the study of the OH vibrations but also for the quantitative determination of the CEC, following the method of Petit *et al*. (1998, 2006). To compare samples quantitatively, spectra were normalized using the main Si−O band near 1000 cm^{-1} as the internal reference.

RESULTS

XRD data

The powder XRD patterns (Figure 1) are characteristic of pure smectites for all samples, except sample Zn200, which also contains willemite and hemimorphite.

For samples synthesized at lower temperatures, a small broad hump is observed between 20 and 50º2θ, indicating a small amount, if any, of residual, X-ray amorphous materials. The XRD patterns of all the samples exhibit asymmetric (*hk*) bands characteristic of a turbostratic stacking of layers. The (*hk*) bands with maximum diffraction intensity located at ~4.5 Å, 2.61−2.64 Å, 1.7 Å, and 1.53 Å, correspond to the 02,11, 13,20, 15,24,31, and 06,33 bands of smectites, respectively. The 13,20 band is relatively intense compared to Mg-smectites, due to the high Zn-scattering factor (Kotochigova and Zucker, 2005). The $d_{06,33}$ values are at 1.53±0.005 Å, characteristic of trioctahedral clay minerals, and are in the same range as those measured by Higashi *et al.* (2002) for synthetic hectorite-like and saponite-like sauconite (1.525 and 1.532 Å, respectively). The $d_{06,33}$ does not vary significantly for the three samples synthesized at lower temperatures, but decreases slightly with increase in synthesis temperature (Table 3).

In air-dried conditions, the d_{001} value decreased with synthesis temperature from 15 Å for sample Zn80 to 10.6 Å for sample Zn200 (Table 3), reflecting a decrease in the mean water content in the interlayer space. Note that in these untreated samples, the interlayer cation can be Zn^{2+} and/or Na^+. For samples synthesized at lower temperatures (<120ºC), the d_{001} values revealed that some Zn^{2+} probably occurred as interlayer cations (two water layers), because Na^+ would lead to a one-water-layer configuration (12 Å), under the given experimental conditions. After ethylene glycol (EG) solvation, the 001

Table 2. Thermal events of the synthetic samples.

Sample	1st endo	2nd endo	1st exo	2nd exo	$\%H_2O$	%OH	%cryst
Zn80	78	550	781	965	8.9	2.7	69
Zn100	83	553	780	955	9.8	2.9	73
Zn120	76	565	781	968	7.2	3.9	101
Zn150	69	575	780	968	6.5	2.4	63
Zn200	63	615	765	952	4.2	2.9	78

endo: endotherm
exo: exotherm
$\%H_2O$: hydration water loss measured by TGA from 20 to 250ºC (wt.%)
%OH: water loss due to dehydroxylation measured by TGA from 250 to 700ºC (wt.%)
%cryst: calculated % of crystallization (see text).

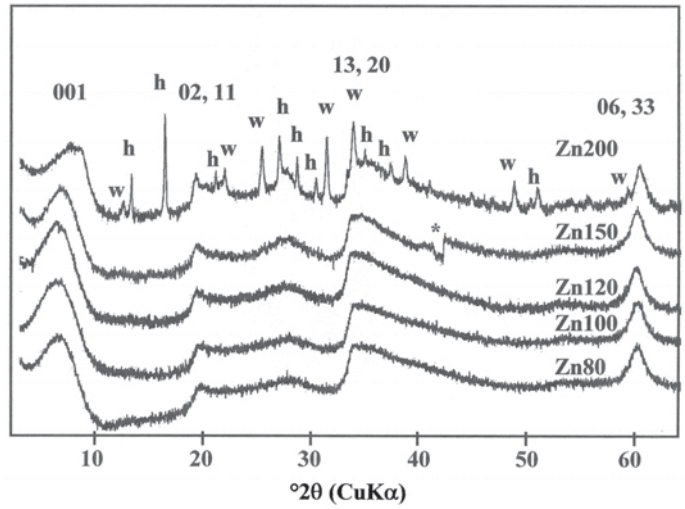

Figure 1. Powder XRD patterns of the synthetic samples described in Table 1. h – hemimorphite; w – willemite; * – instrumental problem.

reflection expanded to 17–18 Å (Table 3), clearly characteristic of smectite-type clays for all samples. The very large swelling for the Zn100 and Zn120 samples may have come from very poor crystallinity, and/or from a possible complex interstratification of layers with different EG intercalation properties. Similar behavior was also observed for natural, trioctahedral, low-charge smectites, and was interpreted as interstratification or the presence of extremely thin particles (Polyak and Güven, 2000; Cuevas *et al.*, 2003; Yeniyol, 2007). After heating at 300ºC for 2 h, Zn200 collapsed to 9.9 Å, while greater spacings were measured for the other samples (Table 3), possibly due to a rapid partial rehydration of smectites under ambient atmosphere. After re-exposure to ethylene glycol of these heated samples, all the samples swelled again, with the same amplitude as before the heat treatment for Zn150 and Zn200, and, to a lesser extent, for the samples synthesized at lower temperatures (Table 3). For the latter samples, the possibility of a partial HK effect with interlayer Zn^{2+} was not excluded (see below).

Thus, the synthesized products apparently are actually Zn-stevensite, with the structural formula $Si_4(Zn_{3-x}\square_x)O_{10}(OH)_2R_a^+$.

After Zn-HK treatment, d_{001} was near 10 Å for all samples, and did not change after EG saturation (Table 3), indicating Zn-talc-like clay. For convenience, the term 'Zn-talc' will be used hereafter instead of the 'Zn-kerolite' term, even though the latter might be more appropriate due to the turbostratically disordered layer stacking observed for the Zn-HK samples (Brindley, 1980).

The successive d_{001} values under several treatments are illustrated in Figure 2 for the Zn150 sample.

Thermal analyses

The DTA curves for all synthetic samples are similar (Figure 3) and exhibit the characteristic features of Zn-smectites with the two typical exothermic peaks at high temperatures (at ~780 and 960ºC) due to successive recrystallizations into Zn_2SiO_4 polymorphs (Faust, 1951). The temperature of the first endotherm, due to dehydration, varied throughout the series, perhaps due to the heterogeneity of the interlayer cations (Na^+, Zn^{2+}) and/or to the dehydration of some residual gel (Table 2). The temperature of the second endothermic peak, due to smectite dehydroxylation, increased regularly from sample Zn80 to sample Zn200, reflecting a greater

Table 3. XRD characterization of samples.

Sample	AD	EG	H	H EG	ZnHK	ZnHK EG	06,33
Zn80	15.0	17.5	12.2	13.5	10.6	10.6	1.533
Zn100	13.9	18.4	12.3	14.1	10.6	10.6	1.533
Zn120	12.8	18.8	11.9	16.0	10.3	10.3	1.535
Zn150	12.3	17.6	11.2	17.5	10.1	10.1	1.530
Zn200	10.6	17.1	9.9	17.1	9.8	9.8	1.525

Position of the 001 reflection for: AD – air-dried preparation; EG – glycolated preparation; H – heated at 300ºC for 2 h; H EG – heated at 300ºC and glycolated; ZnHK – heated at 300ºC overnight after Zn^{2+} exchange; ZnHK EG – ZnHK glycolated; 06,33 – position of the 06,33 reflection. All reflection positions are given in Å.

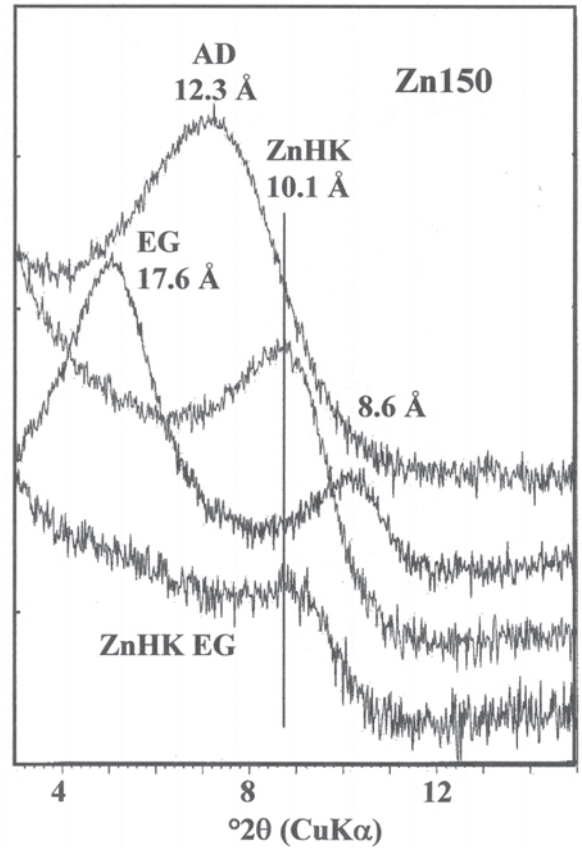

Figure 2. XRD pattern of the oriented clay-aggregate Zn150 synthetic sample. AD – air dried; EG – glycolated; ZnHK – Zn-treated (see text); ZnHK EG – Zn-treated and glycolated,

thermal stability of smectite with increasing synthesis temperature. This is commonly observed for clay syntheses performed under rather low hydrothermal conditions (<250ºC) (Petit, 1990; Decarreau *et al*., 2008). The dehydroxylation temperatures are in a lower range than those measured for natural Zn-smectite (sauconite) (Faust, 1951), but are in the same range as those measured by Higashi *et al.* (2002) for synthetic hectorite-like and saponite-like sauconites.

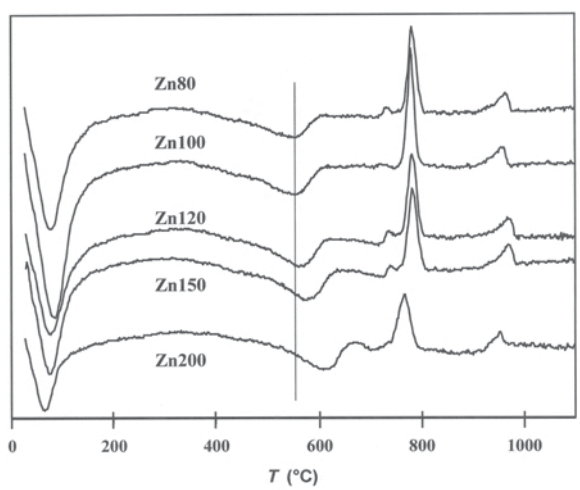

Figure 3. DTA patterns of the synthetic samples.

The rate of smectite crystallization (%cryst, Table 2) can be approximated roughly by comparing the water loss due to dehydroxylation (%OH), measured by TGA, with its calculated theoretical value. The estimated rate of smectite crystallization is relatively high (Table 2). From TGA, only sample Zn120 could be considered as completely pure (initial gel totally transformed into clay). The deviations from 100% are possibly due to either partial transformation of the initial product (and remainder of residual product) and/or the occurrence of impurities (willemite and hemimorphite were detected by XRD for sample Zn200). Deviations from the $Si_4Zn_{(3-x)}O_{10}(OH)_2Zn_x.nH_2O$ theoretical composition assumed for the crystallized smectite are also possible.

Infrared spectroscopy

The IR spectra (Figure 4) of the synthesized samples are very similar to those of synthetic hectorite-like and saponite-like sauconites (Higashi *et al*., 2002). Notably, they show the characteristic νZn_3OH band at 3643 cm^{-1} (Petit, 2005). The width of the 3643 cm^{-1} band tends to decrease when the synthesis temperature increases (Table 4). Another band at ~670 cm^{-1} is characteristic of trioctahedral clays. In the case of Zn-smectites, this band at 662 cm^{-1} is mainly due to δZn_3OH. By analogy with other trioctahedral clays (Decarreau *et al*., 1992), it probably overlaps a lattice vibration ($A_1\nu_2SiO$). For the Zn200 sample, small bands at ~875, 800, and 600 cm^{-1} are due to impurities also detected by XRD.

After LiHK and ZnHK treatments, the spectra varied only slightly. The width of the 3643 cm^{-1} band tended to decrease for LiHK-treated samples and all the more so for ZnHK-treated samples (Table 4). A small shift towards smaller wavenumbers was also observed (Figure 5). The band at 662 cm^{-1} followed the same behavior. In the NIR OH-combination region (Figure 6), the spectra were better resolved (bands are narrower) after HK treatment and all the more so for ZnHK-treated samples. Notably, the band at 4309 cm^{-1}, which can be attributed to $(\nu+\delta)Zn_3OH$, increased for the HK-treated samples.

To determine quantitatively the evolution of CEC after LiHK and ZnHK treatment, the integrated inten-

Table 4. Full width at half height (cm^{-1}) of the νZn_3OH band at 3643 cm^{-1}.

Sample	Untreated	LiHK	ZnHK
Zn80	25	25	24
Zn100	23	23	23
Zn120	24	21	19
Zn150	23	20	16
Zn200	16	13	9

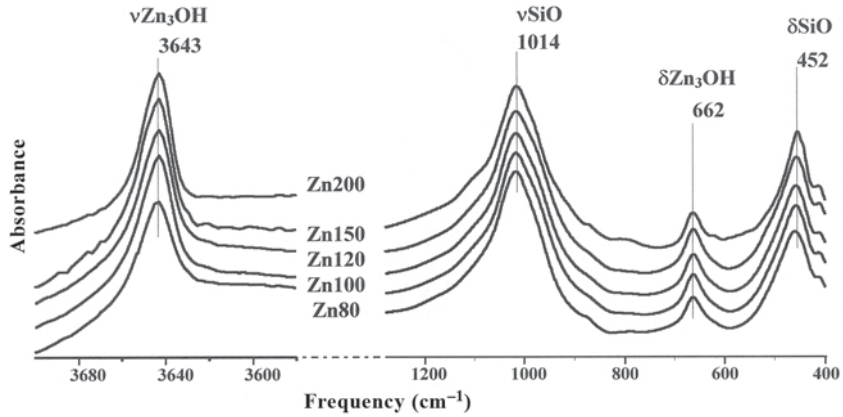

Figure 4. FTIR spectra of the synthetic samples in the mid-infrared region.

sities of the υNH_4^+ band near 1400 cm^{-1} (Figure 5) were measured for the NH_4^+-saturated samples following the method described by Petit *et al*. (1998, 2006). To compare the samples quantitatively, the spectra were normalized using the main Si−O band near 1000 cm^{-1} as the internal reference. Using the CEC measured independently for Zn100 (Table 1), the NH_4^+ contents in arbitrary units were then converted into cmol/kg for all untreated and HK-treated samples (Figure 7). The CEC of sample Zn80 is large (125 cmol/kg) compared to the samples synthesized at greater temperatures (Figure 7), and is typical of smectite. Samples Zn100, Zn120, and Zn200 have relatively small CEC values for smectites (between 43 and 54 cmol/kg) while sample Zn150 has an intermediate CEC value (69 cmol/kg). Note that the CEC obtained for Zn200 (Figure 7) was greater than that measured using the independent method (Table 1). Because the impurities present in Zn200 have very little influence on the IR spectra, the ammonium content which was measured corresponds mainly to clay while the CEC measured independently corresponds to the whole sample. No case can be made for relationships between the CEC values of untreated samples and synthesis temperatures. The LiHK treatment induces a significant decrease in CEC, except for Zn120. Treatment with ZnHK induced a significant decrease in CEC values compared to LiHK treatment, at least for samples Zn80 and Zn150 (Figure 7). For the ZnHK-treated Zn100 and Zn200 samples, the CEC values show a slight decrease compared to LiHK-treated samples, and a significant decrease compared to untreated samples. The CEC value of the ZnHK-treated Zn200 is 13 cmol/kg. Unlike the other samples, the Li- and Zn-HK treatments did not seem to have any influence on the CEC value for sample Zn120.

After NH_4^+ saturation, the NH_4^+ content measured by FTIR corresponded to the CEC value and thus to the total accessible charge (permanent plus variable charges) of the samples. Except for the Zn120 sample, a clear reduction in CEC was observed after Li and Zn-HK treatments. The reduction in CEC value is assumed to correspond to migration of Li^+ or Zn^{2+} into vacant sites.

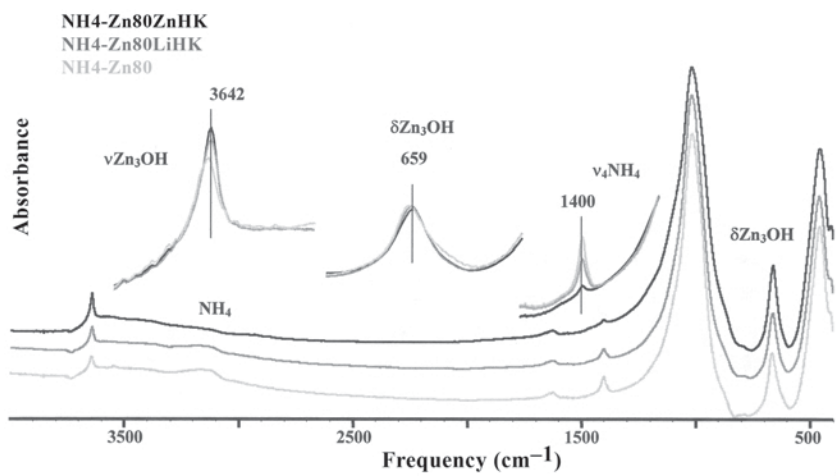

Figure 5. FTIR spectra of the NH_4-saturated Zn80 sample in the mid-infrared region before and after Li- and Zn-HK treatments.

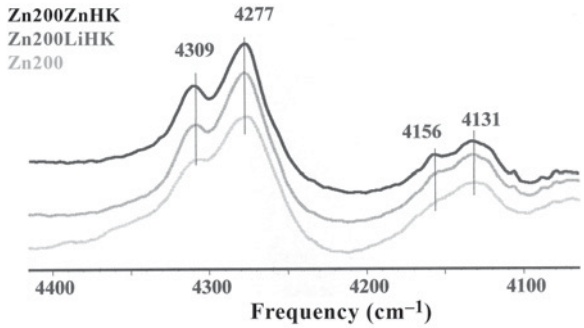

Figure 6. FTIR spectra of the Zn200 sample in the NIR OH combination-band region before and after Li- and Zn-HK treatments.

Thus, after LiHK treatment, the structural formula of the samples can be expressed as $Si_4Zn_{(3-x)}Li_xO_{10}(OH)_2NH^+_{4a}$ with $a = x$, while after ZnHK treatment, the structural formula of the samples can be expressed as $Si_4Zn_3O_{10}(OH)_2$, which corresponds to a Zn-talc mineral. The small amount of ammonium measured by FTIR after ZnHK treatment is then assumed to come essentially from variable charges.

Assuming that the residual charge measured after ZnHK treatment is due to variable charges only, and that Li- and Zn-HK treatments do not disturb significantly crystal edges and the development of variable charge (Righi *et al*., 1998), the CEC value corresponding to permanent charge (CEC_{perm}) of untreated and LiHK samples was recalculated by subtracting the NH^+_4 amounts measured for ZnHK samples from the NH^+_4 amounts measured for untreated and LiHK samples, respectively (Figure 8). Data are also expressed as layer charge, a, per half unit cell ($O_{10}(OH)_2$) following relation 1.

Except for sample Zn80, synthesized stevensites are low-charge smectites. The permanent charge calculated for samples Zn100 and Zn120 is even close to 0. The number of vacancies is thus very small in the synthesized stevensites (half of a).

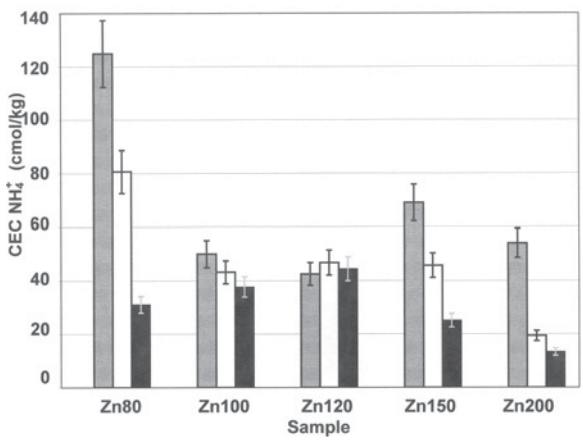

Figure 7. FTIR measurement of the NH^+_4 content expressed as CEC of the NH^+_4-saturated samples. Gray – untreated samples; white – LiHK-treated samples; black – ZnHK-treated samples

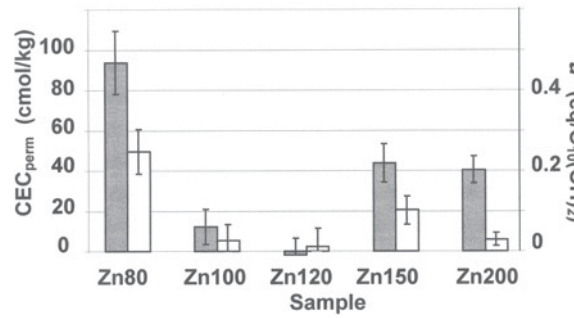

Figure 8. (*left axis*) CEC due to the permanent charge of synthetic samples. (*right axis*) Corresponding layer charge per half unit-cell. Gray – untreated samples; white – LiHK-treated samples.

DISCUSSION AND CONCLUSIONS

Synthesis of Zn-smectites

Pure Zn-smectites can be synthesized from a Si-Zn coprecipitated gel and from 80 to 150ºC within 1 month. At 200ºC, Zn-smectite could also be synthesized, but willemite and hemimorphite admixtures were detected by XRD. These two crystalline Zn silicates are often reported to occur in synthesis experiments in the Zn-Si system (*e.g*. Kloprogge *et al*., 1999). The present results suggest that the increase in synthesis temperature favors the crystallization of impurities, as the only parameter which varies is temperature. This is in accordance with Roy and Mumpton (1956) who suggested that 200ºC is the minimum temperature for the formation of willemite under hydrothermal conditions. However, note that Esquevin (1960) obtained willemite and hemimorphite at temperatures as low as 100ºC. The synthesis and stability relations of silicates in the ZnO-SiO_2 system were studied (Roy and Mumpton, 1956) using gels incubated in the range 130–730ºC (35–276 bar). Pure sauconite was obtained only up to 210ºC. Optimizing the process to synthesize sauconite, hemimorphite, and willemite, Usui *et al*. (1987) found that using active silicic acid prepared by an acid treatment of a clay mineral is the key factor in reducing the synthesis conditions, notably the pressure, in comparison to the Roy and Mumpton (1956) process. Within hours, and at vapor-saturation pressure, sauconite was synthesized (Usui *et al*., 1987). The optimal ZnO/SiO_2 molar ratio to obtain sauconite is 3/4 (*i.e.* stoichiometric ratio); it is less for hemimorphite and willemite. The optimal temperature range is 130–170ºC for sauconite, 150–250ºC for hemimorphite, and >200ºC for willemite. In this study, only one synthesis time was used which was much greater (1 month) than the synthesis time (<1 day) used by Usui *et al*. (1987). Therefore, the use of active laminar silica probably improves the process. The only restriction to this

procedure is that it always introduces some Al into the system. Actually, small amounts of Al from initial clay (silica source) are always present as a residual product associated with the active silica.

According to Usui *et al*. (1987), the upper temperature limit to obtain pure sauconite was found at <200ºC. However, sauconite was easily synthesized at temperatures of <130ºC. The smallest temperature used was 80ºC, and a reasonably well crystallized sauconite was achieved. Moreover, this temperature apparently is not the lower limit and Zn-smectite could probably form at even lower temperatures. Indeed, others (Tiller and Pickering, 1974; Leggett, 1978) observed by means of XRD that Zn-smectite was synthesized under Earth-surface conditions (20ºC, 1 bar) but only after at least 1−2 y. Moreover, in batch experiments at 25ºC for a few days with pre-existing hectorite (Schlegel *et al*., 2001) and montmorillonite (Schlegel and Manceau, 2006), Zn-phyllosilicate neoformation was revealed by EXAFS and solution-chemistry studies. Those authors suggested that the pre-existing clays act as nucleating surfaces promoting crystallization of Zn-kerolite. The ease of Zn-phyllosilicate crystallization is possibly due to the fact that Zn^{2+} cations hydrolyze at near-neutral pH values, promoting polymerization with silicic acid (Mizutani *et al*., 1990). Under hydrothermal conditions, the hydrolysis rate increases and nucleation and growth of smectite can be accelerated. However, the advantage of greater rates of reaction could be offset by the formation of other Zn-silicates with a different stability field, as seen for the 200ºC experiment.

Crystal chemistry of synthesized smectites

From the same initial gel, having the $Si_4Zn_3O_{11}$ composition, a series of Zn-smectites, *i.e.* sauconites, was synthesized at various temperatures (80, 100, 120, 150, and 200ºC). Because Zn could not substitute for Si (at least in such low-temperature minerals), the permanent charge of smectite necessarily comes from octahedral vacancies only. Synthesized sauconites are therefore of stevensite type with the structural formula $Si_4(Zn_{3-x}\square_x)O_{10}(OH)_2R_a^+$. The number of vacant sites per half unit cell ($O_{10}(OH)_2$) ranges from 0.23 (Zn80) to nearly 0 (Zn100 and Zn120). It is ~0.1 for samples Zn150 and Zn200. No obvious relationship exists between the number of vacant sites and the temperature of synthesis. Even for sample Zn80, identifying the Zn_2OH vibration bands by FTIR spectroscopy was not possible. Only a decrease in bandwidth of Zn_3OH was observed with the decrease in charge, which was assumed to be linked to the number of vacant sites. This suggests that such Zn_2OH stretching and bending bands probably occur close to the Zn_3OH bands.

Clay minerals with a very large permanent charge or without any charge swell minimally in water. For montmorillonite, a charge of 0.2 per half unit cell ($O_{10}(OH)_2$) is commonly considered as the lowest limit for full swelling in water (Meier and Nüesch, 1999). Full swelling was not observed for any synthetic samples (see the air-dried value for Zn200, Table 2), although complete swelling was observed for ethylene-glycolated samples, at least for samples Zn80, Zn150, and Zn200. In low-charge smectites, the charge emanates mainly from substitution of divalent for trivalent cations (R^{3+}/R^{2+}) or of monovalent for divalent cations (R^{2+}/Li^+) in octahedral sites giving a charge deficit of 1. In the case of stevensite, however, the local charge deficit is 2, when there is a vacant site. This probably gives specific physicochemical properties to the synthetic stevensites.

HK EFFECT

The possible migration of small interlayer cations into smectite layers under heating has been known for a long time (see Komadel *et al*., 2005). The final position of the fixed cations, deep in the structure of the smectite layer, may vary depending on the crystal chemistry of smectite. For pure montmorillonite (no tetrahedral charge), the so-called 'HK effect' is now generally accepted, by which Li^+ can migrate deep into the structure to the previously vacant octahedral sites. For the migration of divalent cations, such as Zn^{2+}, into smectite layers, no clear supporting data are available. Only a few works have been found on the migration of cations into the structure of trioctahedral smectites, and they focused on hectorites (Jaynes and Bigham, 1987; Jaynes *et al*., 1992). The reasons for this paucity of information are probably: (1) stevensite is not very common in nature; and (2) the LiHK effect has been used widely to distinguish between montmorillonite and beidellite following loss of swelling as seen by XRD (Green-Kelly, 1953, 1955). In the case of stevensite, complete charge compensation by Li^+ is not possible, so charge-induced swelling cannot be completely ruled out. This could not be checked in the present study because no XRD data were obtained due to insufficient amounts of LiHK samples. However, FTIR measurements, using the method of Petit *et al*. (1998), still showed a residual permanent charge after Li^+ fixation (Figures 7 and 8). Plotting the layer charge (corresponding to permanent charge) of LiHK samples *vs.* the layer charge of the untreated samples (Figure 9) revealed that samples Zn80, Zn100, and Zn150 are close to the diagonal line corresponding to $y = 2x$. The assumed change to the structural formula, induced by Li treatment, from $Si_4(Zn_{3-x}\square_x)O_{10}(OH)_2R_a^+$ with $a = 2x$ to $Si_4Zn_{(3-x)}Li_xO_{10}(OH)_2NH_{4a}^+$ with $a = x$ is remarkably well verified for these three samples. For Zn120, the layer charge is very small and the plot is within the uncertainty. For Zn200, the occurrence of silicate impurities may invalidate the FTIR normalization for this sample.

In the case of ZnHK-treated samples, development of non-swelling interlayer spaces after treatment is clearly

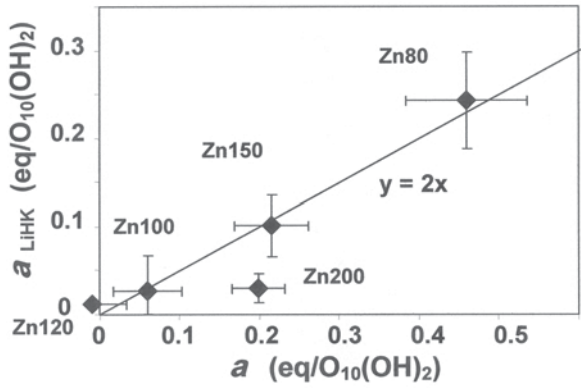

Figure 9. Layer charge (per half unit cell ($O_{10}(OH)_2$)) of LiHK samples *vs.* layer charge of untreated samples.

observed by XRD for all smectites in the series (Table 3). This non-swelling behavior is clearly due to the loss of permanent charge. The ZnHK treatment of Zn-stevensite leads to a talc-like phyllosilicate. This is supported by the decrease in bandwidths of Zn_3OH observed by FTIR spectroscopy after ZnHK treatment, which suggests a more talc-like structure. In case of montmorillonite, the possibility has already been mentioned (Purnell and Lu, 1993; Emmerich *et al.* 1999, 2001) that Zn^{2+} may have migrated within the smectite structure after Zn-HK treatment. In case of the synthetic stevensite, the location of the Zn^{2+} which migrated after ZnHK treatment is actually the previously vacant site.

ACKNOWLEDGMENTS

This paper is dedicated to the memory of Michel Garais who did the careful saturation work.

REFERENCES

Brindley, G.W. (1980) Kerolite and pimelite P. 167 in: *Crystal Structures of Clay Minerals and their X-ray Identification* (G.W. Brindley and G. Brown, editors). Monograph **5**, Mineralogical Society, London.

Cuevas, J., Ramirez, S., Petit, S**.,** Meunier, A., and Leguey, S. (2003) Chemistry of Mg smectites in lacustrine sediments from the Vicálvaro sepiolite deposit, Madrid Neogene basin (Spain). *Clays and Clay Minerals*, **51**, 457–472.

Czímerová, A., Bujdák, J., and Dohrmann, R. (2006) Traditional and novel methods for estimating the layer charge of smectites. *Applied Clay Science*, **34**, 2–13.

Decarreau, A. (1985) Partitioning of divalent transition elements between octahedral sheets of trioctahedral smectites and water. *Geochimica et Cosmochimica Acta*, **44**, 1537–1544.

Decarreau, A., Grauby, O., and Petit, S. (1992) The actual distribution of octahedral cations in 2:1 clay minerals: results from clay synthesis. *Applied Clay Science*, **7**, 147–167.

Decarreau, A., Petit, S., Martin, F., Farges, F., Vieillard, P., and Joussein, J. (2008) Hydrothermal synthesis between 75 and 150ºC of high-charge ferric nontronites. *Clays and Clay Minerals*, **56**, 322–337.

Emmerich, K., Madsen, F.T., and Kahr, G. (1999) Dehydroxylation behavior of heat treated and steam treated homoionic *cis*-vacant montmorillonites. *Clays and Clay Minerals*, **47**, 591–604.

Emmerich, K., Plötze, M., and Kahr, G. (2001) Reversible collapse and Mg^{2+} release of de- and rehydroxylated homoionic *cis*-vacant montmorillonites. *Applied Clay Science*, **19**, 143–154.

Esquevin, J. (1955) Synthèse de montmorillonites zincifères. *Comptes Rendus Académie des Science.*, t. **241**, nº 21, 1485–1486.

Esquevin, J. (1956) Synthèse de phyllites zincifères. *Bulletin du Groupe Français des Argiles*, t**. 8**, nº 3, 23–27.

Esquevin, J. (1960) Les silicates de zinc. Etude de produits de synthèse. *Annales Agronomiques*, **11**, 497–556.

Faust, G.T. (1951) Thermal analysis and X-ray studies of sauconite and of some zinc minerals of the same paragenetic association. *American Mineralogist*, **36**, 795–822.

Genth, F.A. (1875) Mineralogy of Pennsylvania. *Second Geological Survey, Pennsylvania*, p. 120-B.

Greene-Kelly, R. (1953) The identification of montmorillonoids in clay. *Journal of Soil Science*, **4**, 233–247.

Greene-Kelly, R. (1955) Dehydration of montmorillonite minerals. *Mineralogical Magazine*, **30**, 604–615.

Higashi, S., Miki, K., and Komarneni, S. (2002) Hydrothermal synthesis of Zn-smectites. *Clays and Clay Minerals*, **50**, 299–305.

Hofmann U. and Klemen R. (1950) Verlust des Austauschfähigkeit von Lithiumionen an Bentonit durch Erhitzung. *Zeitschrift für Anorganische und Allgemeine Chemie*, **262**, 95–99.

Isaure, M.P., Manceau, A., Geoffroy, N., Laboudigue A., Tamura, N., and Marcus, M. (2005) Zinc mobility and speciation in soil covered by contaminated dredged sediment using micrometer-scale and bulk-averaging X-ray fluorescence, absorption and diffraction techniques. *Geochimica et Cosmochimica Acta*, **69**, 1173–1198.

Jaynes, W.F. and Bigham, J.M. (1987) Charge reduction, octahedral charge, and lithium retention in heated, Li-saturated smectites. *Clays and Clay Minerals*, **35**, 440–448.

Jaynes, W.F., Traina, S.J., Bigham, J.M., and Johnston C.T. (1992) Preparation and characterization of reduced-charge hectorites. *Clays and Clay Minerals*, **40**, 397–404.

Kloprogge, T., Komarneni, S., and Amonette, J. (1999) Synthesis of smectite clay minerals: a critical review. *Clays and Clay Minerals*, **47**, 529–554.

Komadel, P., Madejová, J., and Bujdák, J. (2005) Preparation and properties of reduced-charge smectites – a review. *Clays and Clay Minerals*, **53**, 313–334.

Kotochigova, S.A. and Zucker, D.S. (2005) *X-ray Form Factor, Attenuation and Scattering Tables* (version 2.1). http://physics.nist.gov/ffast (viewed by the author on 05/22/08). National Institute of Standards and Technology, Gaithersburg, Maryland. [Originally published as Chantler, C.T. (1995) *Journal of Physical and Chemical Reference Data*, **24**, 71–643; and Chantler, C.T. (2000) *Journal of Physical and Chemical Reference Data*, **29**, 597–1048.].

Leggett, G. (1978) Interaction of monomeric silicic acid with copper and zinc and chemical changes of the precipitates with aging. *Soil Science Society of America Journal*, **42**, 262–268.

Meier, L.P. and Nüesch, R. (1999) The lower cation exchange capacity limit of montmorillonite. *Journal of Colloid and Interface Science*, **217**, 77–85.

Mench, M.J., Manceau, A., Vangronsveld, J., Clusters, H., and Mocquot, B. (2000) Capacity of soil amendments in lowering the phytoavailability of sludge-borne zinc. *Agronomie*, **20**, 383–397.

Mizutani, T., Fukushima, Y., and Kamigaito, O. (1990) Mechanism of the copolymerization of silicic acid and metal ions in aqueous media. *Bulletin of the Chemical*

Society of Japan, **63**, 618–619.
Petit, S. (1990) Etude cristallochimique de kaolinites ferrifères et cuprifères de synthèse (150–250ºC). PhD thesis, Université de Poitiers, France, 238 pp.
Petit, S. (2005) Crystal-chemistry of talcs: a NIR and MIR spectroscopic approach. Pp. 41–64 in: *The Application of Vibrational Spectroscopy to Clay Minerals and Layered Double Hydroxides* (J.T. Kloprogge, editor). CMS Workshop Lectures, **13**, The Clay Minerals Society, Aurora, Colorado.
Petit, S., Righi, D., Madejová, J., and Decarreau, A. (1998) Layer charge of smectites: quantification and localization using infrared spectroscopy. *Clay Minerals*, **33**, 579–591.
Petit, S., Righi, D., and Madejová, J. (2006) Infrared spectroscopy of NH_4^+-bearing and saturated clay minerals: A review of the study of layer charge. *Applied Clay Science*, **34**, 22–30.
Polyak, V.J. and Güven, N. (2000) Authigenesis of trioctahedral smectite in magnesium-rich carbonate speleothems in Carlsbad cavern and other caves of the Guadalupe mountains, New Mexico. *Clays and Clay Minerals*, **48**, 317–321.
Purnell, J.H., and Lu, Y. (1993) Ionic migration and charge reduction in Ni^{2+}, Co^{2+}, and Zn^{2+}-exchanged Texas montmorillonite. *Catalysis Letters*, **18**, 235–241.
Righi, D., Petit, S., and Bouchet, A., (1993) Characterization of hydroxy-interlayered vermiculite and illite/smectite interstratified minerals from the weathering of chlorite in a cryorthod. *Clays and Clay Minerals*, **41**, 484–495.
Righi, D., Terribile, F., and Petit, S. (1998) Pedogenetic formation of high-charge beidellite in a vertisol of Sardinia (Italy). *Clays and Clay Minerals*, **46**, 167–177.
Ross, C.S. (1946) Sauconite – a clay mineral of the montmorillonite group. *American Mineralogist*, **31**, 411–424.
Roy, D.M. and Mumpton, F.A. (1956) Stability of minerals in the system Zn-SiO_2-H_2O. *Economic Geology*, **51**, 432–443.
Schlegel, M. and Manceau, A. (2006) Evidence for the nucleation and epitaxial growth of Zn phyllosilicate on montmorillonite. *Geochimica et Cosmochimica Acta*, **70**, 901–917.
Schlegel, M., Manceau, A., Charlet, L., Chateigner, D., and Hazemann, J.-L. (2001) Sorption of metal ions on clay minerals. III. Nucleation and epitaxial growth of Zn phyllosilicate on the edges of hectorite. *Geochimica et Cosmochimica Acta*, **65**, 4155–4170.
Tiller, K.G. and Pickering, J.G. (1974) The synthesis of zinc silicates at 20ºC and atmospheric pressure. *Clays and Clay Minerals*, **22**, 409–416.
Usui, K., Sato, T., and Tanaka, M. (1987) Process for the preparation of a synthetic crystalline zinc silicate mineral having a sauconite, willemite or hemimorphite structure. *US patent 4681749*. Date issued: 21 July.
Yeniyol, M. (2007) Characterization of a Mg-rich and low-charge saponite from the Neogene lacustrine basin of Eskisehir, Turkey. *Clay Minerals*, **42**, 541–548.

(*Received 26 November 2007; revised 19 August 2008; Ms. 0103; A.E. P. Komadel*)